Chemical Science

ROYAL SOCIETY OF CHEMISTRY

EDGE ARTICLE

View Article Online
View Journal | View Issue

Cite this: *Chem. Sci.*, 2021, **12**, 8123

All publication charges for this article have been paid for by the Royal Society of Chemistry

Unexpected formation of 1,2- and 1,4-bismethoxyl $Sc_3N@I_h$-C_{80} derivatives *via* regioselective anion addition: an unambiguous structural identification and mechanism study†

Yajing Hu,[a] Yang-Rong Yao,[b] Xuechen Liu,[a] Ao Yu,[a] Xiaoming Xie,[b] Laura Abella,[c] Antonio Rodríguez-Fortea,[c] Josep M. Poblet,[c] Takeshi Akasaka,[a] Ping Peng,[a] Qianyan Zhang,*[b] Su-Yuan Xie,[b] Fang-Fang Li*[a] and Xing Lu*[a]

Received 1st March 2021
Accepted 3rd May 2021

DOI: 10.1039/d1sc01178b

rsc.li/chemical-science

An attempt to achieve heterocyclic cycloadducts of $Sc_3N@I_h$-C_{80} *via* reaction with $Ph_2C{=}O$, PhC≡CPh or PhC≡N in the presence of tetrabutylammonium hydroxide (TBAOH) stored in CH_3OH led to the formation of the unexpected bismethoxyl adducts of $Sc_3N@I_h$-C_{80} (**1** and **2**). Further studies reveal that TBAOH in CH_3OH can boost the CH_3O^- addition efficiently, regardless of the presence of other reagents. Single-crystal X-ray diffraction results firmly assign the molecular structures of **1** and **2** as respective 1,4- and 1,2-bismethoxyl adducts, and reveal unusual relationships between the internal Sc_3N cluster and the addition modes, in addition to the unusual packing mode in view of the orientation of the methoxyl groups. Electrochemical results demonstrate smaller electrochemical gaps for **1** and **2**, relative to that of $Sc_3N@I_h$-C_{80}, confirming their better electroactive properties. Finally, a plausible reaction mechanism involving anion addition and a radical reaction was proposed, presenting new insights into the highly selective reactions between the methoxyl anion and metallofullerenes. **1** and **2** represent the first examples of methoxyl derivatives of metallofullerenes. This work not only presents a novel and facile strategy for the controllable synthesis of alkoxylated metallofullerene derivatives, but also provides new non-cycloadducts for the potential applications of EMFs.

Introduction

Endohedral metallofullerenes (EMFs) are a collection of hybrid molecules with metallic species trapped inside fullerene cages which show novel structures, fascinating properties and promising applications in energy storage/conversion, materials science and biomedicine.[1–4] Exohedral functionalization of EMFs has shown its effectiveness to broaden their application by generation of a variety of useful derivatives. During the last few decades, many synthetic methods have been applied to modify EMFs, among which cycloadditions, such as the Bingel–Hirsch reaction,[5,6] [2+2] benzyne addition,[7,8] the 1,3-dipolar reaction,[9–12] the Diels–Alder reaction,[13] carbene addition[14] and so on,[5,15,16] have been widely utilized. The results show that the chemical properties of EMFs are much different from those of empty fullerenes, resulting in the fact that some chemical reactions which are effective for C_{60} do not work on EMFs.

In contrast, non-cycloadditions of EMFs are relatively rare, and the addition is generally uncontrollable and has low selectivity. Radical reactions, such as trifluoromethylation and benzylation, represent the most effective strategies that afforded singly-bonded EMF-derivatives with identified structures. However, the high reactivity of radical species normally produced a mixture of numerous isomers, bringing challenges in selectivity and the subsequent isolation of pure adducts. For instance, trifluoromethylation of $Sc_3N@I_h$-C_{80}, $Y_2C_2@C_s(6)$-C_{82} and M@C_{60} (M = Gd, La) afforded plenty of isomers for the respective EMFs, *i.e.* $Sc_3N@I_h$-$C_{80}(CF_3)_{2-20}$,[17–19] $Y_2C_2@C_{82}(CF_3)_{16}$ [20] and M@$C_{60}(CF_3)_{3-5}$ (M = Gd, La),[21] respectively, in spite that benzyl radical additions to $Sc_3N@I_h$-C_{80} [22] and $La_2@I_h$-C_{80} [23] showed much better selectivity. Unexpectedly, the Bingel–Hirsch reactions of the paramagnetic M@C_{82}

[a]*State Key Laboratory of Material Processing and Die & Mould Technology, School of Materials Science and Engineering, Huazhong University of Science and Technology, Wuhan, Hubei 430074, China. E-mail: ffli@hust.edu.cn; lux@hust.edu.cn*

[b]*State Key Laboratory for Physical Chemistry of Solid Surfaces, Department of Chemistry, College of Chemistry and Chemical Engineering, Xiamen University, Xiamen 361005, China. E-mail: xmuzhangqy@xmu.edu.cn*

[c]*Departament de Química Física i Inorgànica, Universitat Rovira i Virgili, Marcel·lí Domingo 1, 43007 Tarragona, Spain*

† Electronic supplementary information (ESI) available: *In situ* UV-Vis-NIR spectra of the reaction mixture of $Sc_3N@I_h$-C_{80} with TBAOH (in CH_3OH) in *o*-DCB probed at different times, recycling HPLC profiles of the products, HPLC profiles of pure **1** and **2**, full ^{1}H NMR spectra of **1** and **2**, theoretical optimized structures of **1** and **2**, and optimized *xyz* coordinates of **1** and **2**. CCDC 2049232 and 2049233. For ESI and crystallographic data in CIF or other electronic format see DOI: 10.1039/d1sc01178b

(M = La, Y and so on)[6,24] also afforded singly-bonded adducts, and Lewis acid–base pairs of $Sc_3N@I_h$-C_{80}/$Lu_2@C_{82}$ and N-heterocyclic carbenes commonly bear the singly-bonded nature.[25,26] Additionally, the η^1-complex of $Y@C_{2v}(9)$-$C_{82}Re(CO)_5$ stands as an example with a metal–carbon single bond.[27] However, each of the above strategies requires a specific category of EMFs. For example, the Bingel–Hirsch reactions of diamagnetic EMFs always produce cycloadducts and Lewis acid–base pairs of mono-EMFs have never been obtained. Accordingly, it is currently urgent and meaningful to search for new synthetic methods to achieve non-cycloadducts of EMFs in a controllable manner so as to obtain useful compounds with novel structures and fascinating properties.

Herein, we report the unexpected addition of the methoxyl anion to $Sc_3N@I_h$-C_{80} *via* reaction with the methanol solution of tetrabutylammonium hydroxide (TBAOH) which produced the methoxyl anion (CH_3O^-) *in situ*. Only two derivatives are obtained (**1** and **2**), whose structures have been established by single-crystal X-ray diffraction as 1,4- and 1,2-bismethoxyl adducts, respectively. Further studies reveal an anion-radical relay mechanism for the reaction process. To the best of our knowledge, this is the first report on alkoxylated metallofullerenes and the current method differs from those available for the alkoxylation of fullerenes, which provide new insights into the controlled synthesis and formation mechanism of alkoxyl metallofullerene derivatives.

Results and discussion

In fact, our first attempt was to achieve heterocyclic cycloadducts of $Sc_3N@I_h$-C_{80} through the reaction with $Ph_2C{=}O$, PhC≡CPh or PhC≡N in the presence of TBAOH, following the procedures for C_{60} previously reported by Gao and coworkers.[28] 3 mg $Sc_3N@I_h$-C_{80} was dissolved in 10 ml anhydrous *o*-DCB, and then 10 equivalent of TBAOH (stored in CH_3OH) was added into the solution, the color of which rapidly changed from light brown to dark green (Fig. S1, ESI†). The *in situ* UV-Vis-NIR spectra of the reaction mixture in Fig. S1† showed that the absorption of $Sc_3N@I_h$-C_{80} is red-shifted from 371 to 391 nm, and a new peak appears at about 568 nm, indicating the formation of an anionic intermediate. 100 equivalent of $Ph_2C{=}O$, PhC≡CPh or PhC≡N was then added into the green solution which was quenched by adding 50 equivalent of I_2 after stirring for 2 h. The obtained solid products from all three reactions were dissolved in toluene and analyzed by HPLC (Fig. 1a–c). To our surprise, the reactions do not afford any cycloadducts which have been found for C_{60} (according to mass spectrum data). As a matter of fact, we eventually realized that $Ph_2C{=}O$, PhC≡CPh or PhC≡N did not participate in the reaction as we expected. Therefore, the reaction of $Sc_3N@I_h$-C_{80} and the CH_3OH solution of TBAOH without the addition of $Ph_2C{=}O$, PhC≡CPh or PhC≡N was conducted according to the same procedure as described above (Scheme 1, Fig. 1d). As shown in Fig. 1, the HPLC profiles of the reaction mixtures, either with or without $Ph_2C{=}O$/PhC≡CPh/PhC≡N, showed that the adduct peaks emerged at around 32 min after stirring for 2 hours. Further

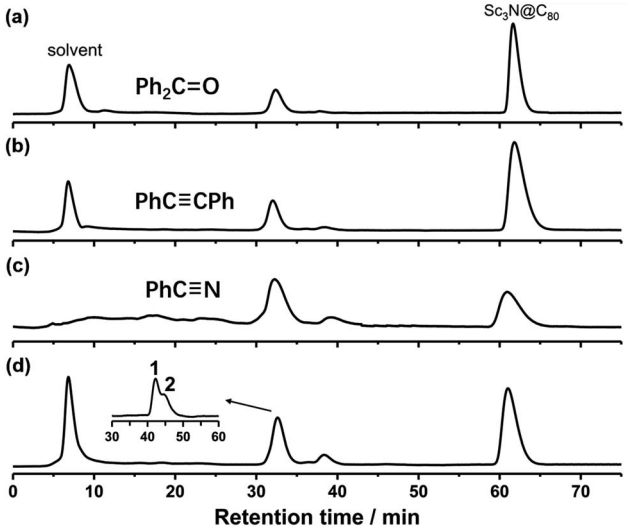

Fig. 1 HPLC profiles of the reaction mixtures containing *o*-DCB solution of $Sc_3N@I_h$-C_{80} and CH_3OH solution of TBAOH with (a) $Ph_2C{=}O$, (b) PhC≡CPh, or (c) PhC≡N and (d) without $Ph_2C{=}O$, PhC≡CPh or PhC≡N. Conditions: Buckyprep column (φ 10 × 250 mm); eluent: toluene, 3 ml min^{-1}. Inset in (d): HPLC profile of the products isolated from the Buckyprep column. Conditions: 5PBB column (φ 10 × 250 mm); eluent: toluene, 5 ml min^{-1}.

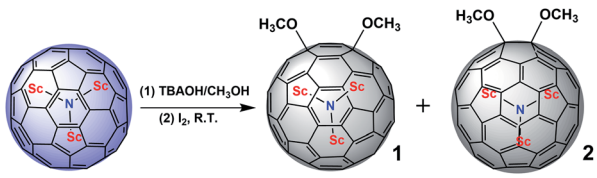

Scheme 1 Reaction of $Sc_3N@I_h$-C_{80} with a methanol solution of TBAOH in *o*-DCB at room temperature, forming the unexpected bismethoxyl derivatives **1** and **2**.

separation gave the pure isomers of **1** and **2** (Fig. S2, ESI†), which have singly-bonded structures (*vide infra*).

1 and **2** are fully characterized by MALDI-TOF MS, NMR, Vis-NIR spectroscopy and single-crystal X-ray diffraction. Fig. 2 displays the mass spectra of **1** and **2** where the peaks at around *m*/*z* 1170.6 correspond to the dimethoxylated adducts $Sc_3N@I_h$-$C_{80}(OCH_3)_2$. The peaks at around 1139.6 and 1108.6 are ascribed to the fragments of $Sc_3N@I_h$-$C_{80}(OCH_3)$ and $Sc_3N@I_h$-C_{80} due to the loss of one or two OCH_3 groups, respectively, confirming the successful attachment of two methoxyl groups on to $Sc_3N@I_h$-C_{80}.

^{1}H NMR spectra (Fig. 3a) provide additional structural features of **1** and **2**. Only one single signal for the two OCH_3 groups in either **1** or **2** is observed, in detail, 3.76 ppm in **1** and 3.84 ppm in **2**, indicative of the highly symmetric placement of the two equivalent OCH_3 groups. Since there are more than 40 possible isomers for $Sc_3N@I_h$-C_{80} bisadducts, the formation of merely two derivatives reveals high regioselectivity. The ^{13}C NMR spectrum of product **1** is shown in Fig. 3b. 38 (including one doublet signal) resonances for the 78 sp^2 I_h-C_{80} cage-carbons are detected from 120.26 to 170.56 ppm, confirming

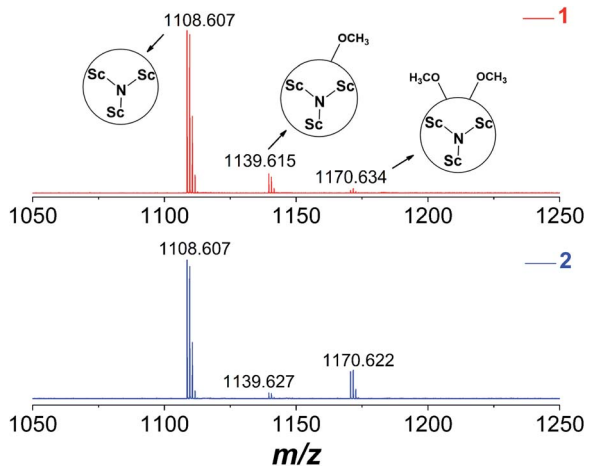

Fig. 2 MALDI-TOF mass spectra of **1** and **2**.

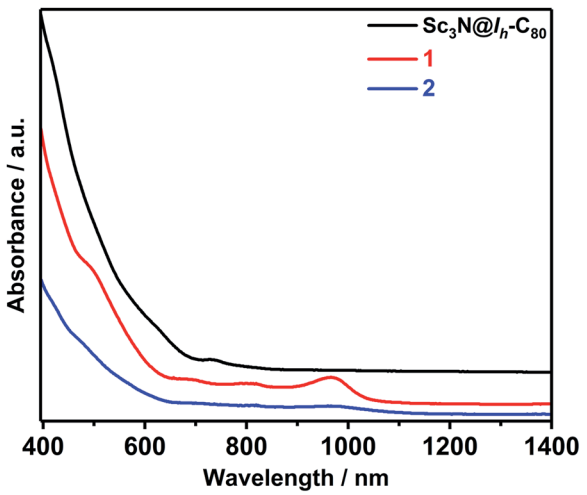

Fig. 4 Vis-NIR spectra of $Sc_3N@I_h$-C_{80}, **1** and **2** in CS_2.

a symmetrical addition pattern of **1**. Resonance for the two sp^3 I_h-C_{80} cage-carbons bonded to the OCH_3 groups appears at 53.76 ppm, while the peak for the two sp^3 OCH_3 carbons appears at 29.15 ppm. Although, the ^{13}C NMR data collection of **2** was not successful due to its relatively low yield, the ^1H NMR spectra of the two products could alternatively elucidate the symmetry of the products, and its X-ray structure provided the absolute structure.

Vis-NIR spectroscopy is a diagnostic tool to estimate the addition position on fullerenes, especially for the highly symmetric C_{60} and $Sc_3N@C_{80}$ cages. Fig. 4 shows the absorption spectra of **1** and **2**. The characteristic peak at 968 nm of **1** is very similar to those of the previously reported 1,4-$Sc_3N@C_{80}(CH_2Ph)_2$ (898 nm)[22] and 1,4-$Sc_3N@C_{80}(CF_3)_2$ (920 nm),[17] suggesting a 1,4-addition pattern. However the absorption curve of **2** is analogous to those of the [5,6]-adducts of $Sc_3N@C_{80}$,[7,8,29] indicative of a 1,2-[5,6]-fashion.

Finally, the molecular structures of **1** and **2** are unambiguously established by single crystal X-ray diffraction. The co-crystals of **[1]·2DPC** and **2[2]·4DPC·2toluene** were obtained by slow evaporation of the toluene/CS_2 solution of the corresponding derivatives and decapyrrylcorannulene (DPC).[30] Both crystals fall into the $P\bar{1}$ space group with variations in the asymmetric unit. **1** shows disorder of both the C_{80} cage and the Sc_3N cluster. Two orientations of the C_{80} cage with equal occupancy and four orientations of the Sc_3N cluster with occupancies of 0.40, 0.35, 0.15 and 0.10 are observed. Interestingly, the C_{80} cage of **2** is highly ordered and only two positions of the Sc_3N cluster with occupancies of 0.82 and 0.18, respectively, are presented.

Fig. 5 shows the molecular structures of **1** and **2** with only the major components together with the cocrystallized DPC molecules. The pairs of DPC and **1** or **2** are assembled into a similar V-shaped configuration with an angle of 61.28° for **[1]·2DPC** (Fig. 5a) and 61.86° for **[2]·2DPC** (Fig. 5b). The distance between the centroid of the C_{80} cage and the central five-membered ring of DPC is 7.313 and 7.308 Å for **1** and 7.382 and 7.313 Å for **2**. The cage-plane distance in **1** and **2** is *ca.* 3.3–3.6 Å, indicating π–π interactions between the fullerene cages and DPC.

It is rather evident that two OCH_3 groups are located at the *para*-position of a six-membered ring, *i.e.*, 1,4-bisaddition on [566]-carbons in **1**, while in **2** are on a [5,6]-ring junction, namely, 1,2-bisaddition. It is noteworthy that the addition

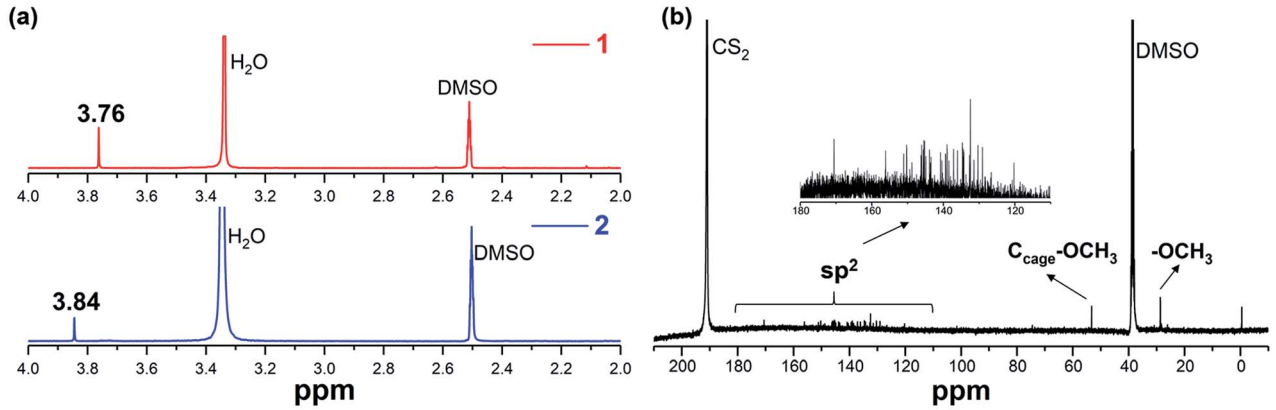

Fig. 3 (a) ^1H NMR spectra of **1** and **2** and (b) ^{13}C NMR spectrum of **1** recorded in CS_2 with DMSO-d_6 as the external lock solvent.

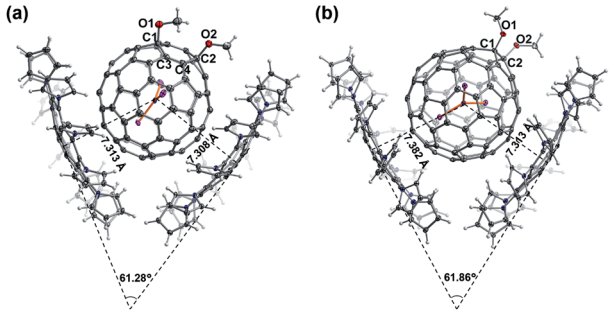

Fig. 5 Single crystal X-ray structures of co-crystals **[1]·2DPC** (a) and **[2]·2DPC** (b) with thermal ellipsoids at the 10% probability level. Only the major cage and the major Sc_3N site are shown. The solvent molecules are omitted for clarity.

patterns show somehow influence on the orientation of the inner cluster. The planar Sc_3N cluster in **1** is orthogonal with the plane crossing the sites of addition, namely, C1–O1–O2–C2, but the metal cluster in **2** is nearly parallel to the plane of C1–O1–O2–C2. Thus, it is proposed that exohedral modification, even merely the addition pattern of bisaddition, is practical to control the cluster orientation.

Notably, the conformations of the two OCH_3 groups in **1** and **2** also differ significantly. The two OCH_3 groups in **1** are unexpectedly arranged towards the same direction, which is unusual and different from the situations observed in the previously reported 1,4-$Sc_3N@C_{80}(CH_2Ph)_2$ and 1,4-$Sc_3N@C_{80}(CF_3)_2$ where the two addition groups are aligned in the opposite position to release steric hindrance.[17,22] We speculate that only the intermolecular steric effect between DPC and **1**, instead of any electronic influence, is responsible for the abnormal alignment of the two OCH_3 groups since there are no C–H$\cdots\pi$ interactions between OCH_3 and DPC.

The packing mode of **[1]·2DPC** (Fig. 6a) reveals that one of the OCH_3 groups (labeled as A) points to three DPC molecules with long intermolecular distances (red circle). Accordingly, the other OCH_3 group (labeled as B) is not allowed to point to the opposite position relative to group A, because it will cause large steric hindrance with the other two adjacent DPC molecules. Besides, the addition pattern of the two OCH_3 groups in **2** is also abnormal since they show a back-and-forth arrangement to decrease both the intramolecular and intermolecular repulsive forces. One OCH_3 group is trapped into the cavity of two DPC molecules (red circle in Fig. 6b) so that the other OCH_3 group can only choose the back orientation, facing three DPC molecules without obvious C–H$\cdots\pi$ interactions. It is thus concluded that the abnormal configurations of the two OCH_3 groups in both **1** and **2** are possibly caused by the intermolecular steric effects of the cocrystallized DPC molecules, which is proved by our theoretical calculations. The optimized structures of **1** and **2** without DPC show that the two OCH_3 are arranged oppositely (Fig. S4, ESI†). In addition, both **1** and **2** are aligned with DPC molecules to form a one-dimensional zigzag supramolecular chain along the *c* and *b* axis, respectively. The fullerenes are arranged in a head-to-tail mode in the packing structures of **1** (along the *b* axis) and **2** (along the *c* axis), respectively (Fig. 6).

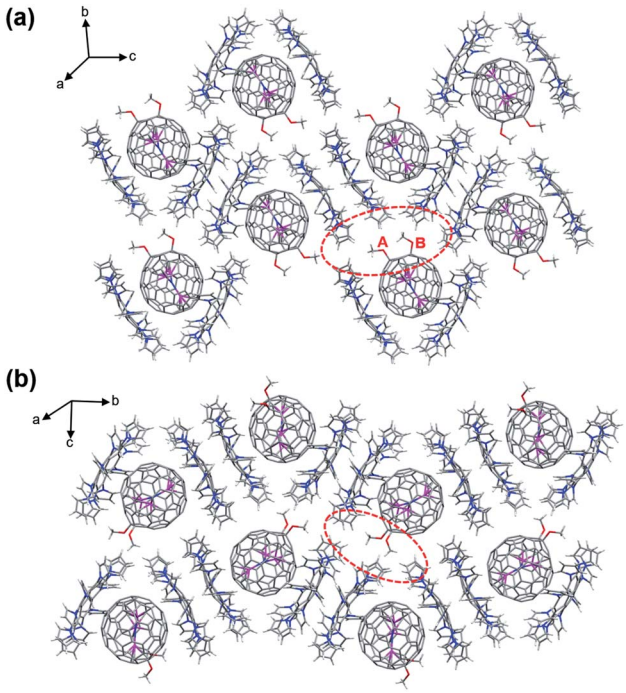

Fig. 6 Packing structures of **[1]·2DPC** (a) and **[2]·2DPC** (b). Only one cage orientation and the major Sc_3N cluster are shown and the solvent molecules are omitted for clarity.

The electrochemical properties of **1** and **2** are studied by cyclic voltammetry (CV) and the results are listed in Fig. 7 and Table 1. The 1,4-adduct **1** displays two irreversible oxidations at +0.40 and +0.59 V and three reversible reductions at −1.17, −1.33 and −1.74 V, respectively, a behavior slightly different from that of the 1,4-$Sc_3N@I_h$-$C_{80}(CF_3)_2$ which displays only one reversible anodic process.[17] Similarly, the 1,2-bisadduct **2** also

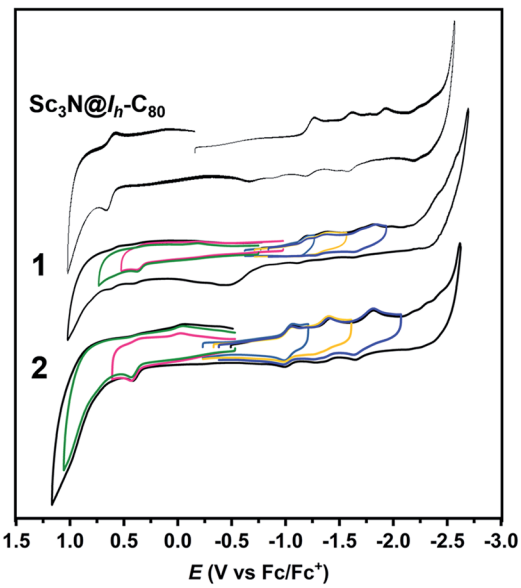

Fig. 7 Cyclic voltammograms of $Sc_3N@I_h$-C_{80}, **1** and **2** recorded in a 0.05 M solution of $TBAPF_6$ in *o*-DCB at a scan rate of 100 mV s^{-1}.

Table 1 Redox potentials of $Sc_3N@I_h$-C_{80} and compounds **1** and **2** *versus* Fc/Fc^+

	$E^{+/2+}$ [V]	$E^{0/+}$ [V]	$E^{0/-}$ [V]	$E^{-/2-}$ [V]	$E^{2-/3+}$ [V]	E_{gap} [V]
$Sc_3N@I_h$-C_{80}		+0.62[b]	−1.26[a]	−1.62[a]	−1.91[a]	1.88
1	+0.59[a]	+0.40[a]	−1.17[b]	−1.33[b]	−1.74[b]	1.57
2	+0.98[a]	+0.43[a]	−1.03[b]	−1.40[b]	−1.72[b]	1.46

[a] Peak potentials. [b] Reversible process.

exhibits two irreversible oxidations at +0.43 and +0.98 V and three reversible reductions at −1.03, −1.40 and −1.72 V, respectively, which is similar to those of the previous reported $Sc_3N@I_h$-C_{80} [5,6]-monoadducts.[7,31,32] Compared with the corresponding redox potentials of pristine $Sc_3N@I_h$-C_{80} (Table 1), the first reduction potentials of **1** and **2** are less negative and their first oxidation potentials are less positive, resulting in smaller electrochemical gaps of the derivatives (1.57 V for **1** and 1.46 V for **2**) than that of $Sc_3N@I_h$-C_{80} (1.88 V) and accordingly higher reactivities, which are beneficial to their future application in photovoltaics and electronics.

Currently, conversion of halofullerenes to alkoxy fullerenes by substituting Cl/Br groups is the most common approach to obtain alkoxy fullerenes,[33–39] which is a complex and multi-step process, requiring the synthesis of halofullerenes first. However, neither halo-EMFs nor alkoxyl-EMFs have been reported due to the unrecognized chemical properties of EMFs. Accordingly, our finding presents a novel solution to the controllable synthesis of alkoxylated fullerene derivatives. We then try to understand the reaction mechanism of this unexpected bis-methoxylation process.

In fact, our initial purpose was to synthesize heterocyclic cycloadducts of $Sc_3N@I_h$-C_{80} following the method reported by Gao and co-workers where C_{60}, tetrabutylammonium hydroxide (TBAOH) and benzonitrile (PhCN) were involved.[28] In the case of C_{60}, OH^- from TBAOH acts as an oxygen nucleophile to form a dianionic intermediate $C_{60}{}^-$–O^- which then attacks the C≡N triple bond of PhCN to produce an O,N-heterocyclic adduct. However, the same process does not occur on $Sc_3N@I_h$-C_{80} even when the more reactive $Ph_2C{=}O$, PhC≡CPh or PhCN were used, and no any cycloadducts have been detected in the reaction mixture, indicating that the reaction mode was changed by the Sc_3N cluster.

Based on the experimental facts, we propose an anion-radical relay mechanism for the formation of **1** and **2** (Scheme 2). First, TBAOH, as a strong organic base, deprotonates CH_3OH to generate CH_3O^- in the less polar solvent *o*-DCB. Due to the better miscibility of CH_3OH with *o*-DCB than TBAOH, CH_3O^- prevails in the addition to $Sc_3N@C_{80}$ over OH^- (from TBAOH) in the *o*-DCB solution. Then, the monoanion $[Sc_3N@C_{80}(OCH_3)]^-$ is oxidized to the $[Sc_3N@C_{80}(OCH_3)]^{\bullet}$ radical by I_2 which accepts another CH_3O^- to form the dimethoxyfullerene anion $[Sc_3N@C_{80}(OCH_3)_2]^-$. Final oxidation by I_2 gives the final products of $Sc_3N@C_{80}(OCH_3)_2$ with either 1,2- or 1,4-addition patterns. This anion radical relay process ensures the high selectivity and controllability of the reaction. The possibility of forming dianionic methoxyfullerene intermediates before I_2-oxidation could be reasonably excluded by considering the high charge density on the cage and thus the low stability in solution.

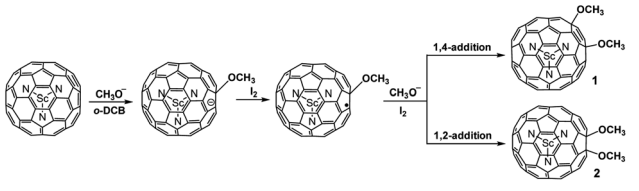

Scheme 2 Plausible mechanism of the reaction between $Sc_3N@I_h$-C_{80} and TBAOH/CH_3OH in *o*-DCB.

Most electrochemical reactions involving fullerenes or EMF anions follow the "electron transfer-S_N2 reaction" mechanism.[15,16,40] But there is an exception that the electrochemical reaction of a C_{60} derivative reported by Wang's group follows a "stepwise one-electron reduction and protonation" mechanism, in which the monoanionic intermediate was protonated to generate a free radical on the adjacent carbon.[41] The anion radical relay mechanism of methoxylation of $Sc_3N@C_{80}$ follows the electron transfer process proposed in most electrochemical reactions, but is followed by a process in which the anion is directly oxidized to a free radical.

It is known that the hydroxylation reactions of C_{60} and EMFs were conducted by adding strong base NaOH containing TBAOH as a catalyst to the fullerene solution. The OH^- as a nucleophile was added on the fullerene cage and a negative charge was transferred to the carbon cage. Then, the negative charge was neutralized by H^+ addition.[42,43] Moreover, the reactions proceeded in an uncontrolled manner and generated multi-hydroxy derivatives,[42,43] which makes it difficult to perform unambiguous structural identification. However, in our methoxylation reaction of $Sc_3N@C_{80}$, TBAOH (1.0 M in CH_3OH) acted as a deprotonating agent of CH_3OH rather than a nucleophile to participate in the reaction. Therefore, no hydroxyl derivatives were formed, and instead methoxyl derivatives were formed. More importantly, the methoxylation reaction was carried out in a controlled manner. The unique stepwise addition pattern ensured high regioselectivity of the reaction, thereby promoting the separation, purification and structure determination of the products.

Conclusions

In summary, we discovered for the first time that the methoxyl anion (CH_3O^-) could react with $Sc_3N@I_h$-C_{80} in a highly regioselective manner to produce merely two isomers (1,4-adduct for **1** and 1,2-adduct for **2**) out of more than 40 possibilities, representing the first examples of bismethoxyl derivatives of metallofullerenes. Their molecular structures and electrochemical properties are systematically investigated by a collection of experimental techniques. Based on the experimental evidence, an anion-radical relay mechanism for the formation of **1** and **2** has been proposed which is highly dependent on the type of solvents used, revealing an unprecedented reaction process for metallofullerenes. Significantly, we provide a facile synthetic

strategy for alkoxylation of metallofullerenes in a highly regioselective manner under mild conditions.

Experimental

Materials and methods

$Sc_3N@I_h$-C_{80} was synthesized by the direct current arc discharge method and isolated by high performance liquid chromatography (HPLC).[7] Tetrabutylammonium hydroxide (TBAOH) (1.0 M in CH_3OH), anhydrous *o*-DCB, $Ph_2C{=}O$, $PhC{\equiv}CPh$, anhydrous $PhC{\equiv}N$, I_2, toluene, DMSO-d_6 and CS_2 were purchased from Sigma-Aldrich and were used as received. Tetra-*n*-butylammonium-hexafluorophosphate ($TBAPF_6$) was recrystallized from absolute ethanol and dried in a vacuum before use. The purity of the products **1** and **2** was verified by HPLC (LabocACE LC-5060, Japan Analytical Industry Co., Ltd., Japan) equipped with Buckyprep and 5PBB columns with toluene as the eluent. Vis-NIR spectra were recorded using a SHIMADZU UV-3600 spectrophotometer. MALDI-TOF MS was conducted on a Bruker autoflex speed mass spectrometer. The ^{1}H NMR spectra were recorded using a Bruker Ascend™ 600 MHz NMR spectrometer. The ^{13}C NMR spectrum was recorded using a Bruker Ascend™ 400 MHz NMR spectrometer. CV studies were conducted in a one-compartment cell connected to a CHI 760E workstation in a solution of *o*-DCB containing 0.05 M $TBAPF_6$. A 2 mm diameter glassy carbon disk was used as the working electrode, and a Pt wire and a Ag wire as the counter and pseudo-reference electrodes, respectively. Ferrocene (Fc) was added to the solution at the end of each experiment as an internal standard. All reactions were carried out in a glove box with Ar protection.

Synthetic procedures of 1 and 2

3 mg $Sc_3N@I_h$-C_{80} was dissolved in 10 ml anhydrous *o*-DCB, and then 10 equivalent of TBAOH (stored in CH_3OH) was added into the solution, which was quenched by the addition of 50 equivalent of I_2 after stirring for 2 h. The obtained solid products from the reaction were dissolved in toluene and analyzed by HPLC (Fig. 1d). Products **1** and **2** were isolated and purified by two-step HPLC.

Compound **1** (yield: 29.7%): MALDI-TOF MS (negative ionization mode): *m*/*z* 1170.634; Vis-NIR 968 nm; ^{1}H NMR (600 MHz, CS_2/DMSO, 25 °C, TMS): $\delta = 3.76$ ppm (s, 6H, –OCH_3). ^{13}C NMR (400 MHz, CS_2/DMSO, 25 °C, TMS): $\delta = 170.56$ (2C), 163.87 (2C), 156.13 (2C), 151.09 (2C), 150.25 (2C), 149.37 (2C), 148.79 (2C), 146.27 (2C), 146.05 (2C), 145.66 (2C), 145.45 (2C), 145.24 (2C), 144.90 (2C), 143.89 (2C), 143.63 (2C), 143.44 (2C), 140.82 (2C), 140.42 (2C), 140.27 (2C), 139.40 (2C), 139.33 (2C), 138.98 (2C), 138.93 (2C), 138.47 (2C), 137.13 (2C), 136.05 (2C), 134.67 (2C), 134.59 (2C), 134.47 (2C), 134.33 (2C), 134.25 (2C), 132.72 (2C), 132.45 (4C), 131.45 (2C), 130.32 (2C), 129.12 (2C), 126.60 (2C), 120.26 (2C), 53.76 (2C, sp^3, C_{cage}–OCH_3), 29.15 ppm (2C, sp^3, –OCH_3).

Compound **2** (yield: 10.9%): MALDI-TOF MS (negative ionization mode): *m*/*z* 1170.622; Vis-NIR 992 nm; ^{1}H NMR (600 MHz, CS_2/DMSO, 25 °C, TMS): $\delta = 3.84$ ppm (s, 6H, –OCH_3).

Single crystal X-ray crystallography

0.5 mg of **1** was dissolved in 0.5 ml carbon disulfide in a 5.0 ml centrifuge tube. Then, a toluene solution of DPC was added into the tube. The mixed solution, in which DPC and fullerene have a molar ratio of 2 : 1, was kept undisturbed at room temperature for slow evaporation. After two weeks, black sheet-like crystals were formed. A crystal of 0.12 mm × 0.08 mm × 0.01 mm dimension was mounted in the 100 K nitrogen cold stream on an XtaLAB PRO MM007HF diffractometer with Cu-Kα radiation (λ = 1.5406 Å). The CrystalClear software package (Rigaku) was used for data collection, cell refinement, and data reduction. The crystal structure of **1** was solved by direct methods and refined by the full-matrix method based on F^2 using the SHELXLTL software package.[44] All the non-hydrogen atoms were refined anisotropically and the positions of the hydrogen atoms were generated geometrically.

Crystal data of **[1]·2DPC** (CCDC-2049232): $C_{202}H_{86}N_{21}O_2Sc_3$, $M_w = 2973.79$ amu, triclinic, $P\bar{1}$, $a = 14.4545(3)$ Å, $b = 17.5373(5)$ Å, $c = 30.8351(5)$ Å, $\alpha = 96.365(2)°$, $\beta = 101.776(2)°$, $\gamma = 96.180(2)°$, $V = 7536.3(3)$ Å^3, $T = 100$ K, $Z = 2$, R indices (all data) $R_1 = 0.1158$, w$R_2 = 0.3470$, GOF (on F^2) = 1.045.

Black sheet-like crystals of **2** were obtained similarly. Crystallographic characterization of a piece of cocrystal (0.03 mm × 0.03 mm × 0.02 mm) was performed at 100 K by using synchrotron radiation (0.65250 Å) with a MarCCD detector at the beamline BL17B station of Shanghai Synchrotron Radiation Facility. The multiscan method was used for absorption corrections. The crystal structure of **2** was solved by the direct methods and refined by the full-matrix method based on F^2 using the SHELXLTL software package.[44] All the non-hydrogen atoms were refined anisotropically and the positions of the hydrogen atoms were generated geometrically.

Crystal data of **[2]·2DPC·toluene** (CCDC-2049233): $C_{209}H_{94}N_{21}O_2Sc_3$, M_w = 3065.93 amu, triclinic, $P\bar{1}$, a = 14.4947(8) Å, $b = 31.8931(18)$ Å, $c = 32.660(2)$ Å, $\alpha = 91.077(1)°$, $\beta = 95.165(2)°$, $\gamma = 101.899(1)°$, $V = 14\ 703.0(15)$ Å^3, $T = 100$ K, Z = 4, R indices (all data) $R_1 = 0.1613$, w$R_2 = 0.4173$, GOF (on F^2) = 1.025.

Computational details

All computations were performed using the density functional theory (DFT) methodology with the ADF 2016 program. The exchange-correlation functionals of Becke and Perdew (BP86) and the Slater triple-ζ + polarization (TZP) basis sets were selected for geometry optimizations.[45,46]

Author contributions

Y. Hu: data collection, writing-original draft; Y.-R. Yao: crystal structure analysis; X. Liu and A. Yu: synthesis of raw materials; X. Xie, Q. Zhang and S.-Y. Xie: synthesis of DPC; L. Abella, A. Rodríguez-Fortea, and J. M. Poblet: theoretical calculations; T. Akasaka: writing-commenting and editing; P. Peng: project management; F.-F. Li: conceptualization, supervision, writing-commenting and editing; X. Lu: conceptualization, writing-commenting and editing.

Conflicts of interest

The authors declare no conflict of interest.

Acknowledgements

Financial support from the National Natural Science Foundation of China (Grant No. 22071070, 21925104, 21971077, 51772111 and 21672076) and the Spanish Ministry of Science (grant CTQ2017-87269-P) is gratefully acknowledged.

Notes and references

1 S. Yang, T. Wei and F. Jin, *Chem. Soc. Rev.*, 2017, **46**, 5005–5058.
2 K. Wang, X. Liu, R. Huang, C. Wu, D. Yang, X. Hu, X. Jiang, J. C. Duchamp, H. Dorn and S. Priya, *ACS Energy Lett.*, 2019, **4**, 1852–1861.
3 K. Zhang, C. Wang, M. Zhang, Z. Bai, F.-F. Xie, Y.-Z. Tan, Y. Guo, K.-J. Hu, L. Cao, S. Zhang, X. Tu, D. Pan, L. Kang, J. Chen, P. Wu, X. Wang, J. Wang, J. Liu, Y. Song, G. Wang, F. Song, W. Ji, S.-Y. Xie, S.-F. Shi, M. A. Reed and B. Wang, *Nat. Nanotechnol.*, 2020, **15**, 1019–1024.
4 T. Wang and C. Wang, *Small*, 2019, **15**, 1901522.
5 Y. Hu, A. Solé-Daura, Y.-R. Yao, X. Liu, S. Liu, A. Yu, P. Peng, J. M. Poblet, A. Rodríguez-Fortea, L. Echegoyen and F.-F. Li, *Chem.–Eur. J.*, 2020, **26**, 1748–1753.
6 W. Shen, L. Yang, B. Li, P. Jin, B. Yu, H. Cong, T. Akasaka and X. Lu, *Chem. Commun.*, 2020, **56**, 14357–14360.
7 F.-F. Li, J. R. Pinzón, B. Q. Mercado, M. M. Olmstead, A. L. Balch and L. Echegoyen, *J. Am. Chem. Soc.*, 2011, **133**, 1563–1571.
8 G.-W. Wang, T.-X. Liu, M. Jiao, N. Wang, S.-E. Zhu, C. Chen, S. Yang, F. L. Bowles, C. M. Beavers, M. M. Olmstead, B. Q. Mercado and A. L. Balch, *Angew. Chem., Int. Ed.*, 2011, **50**, 4658–4662.
9 O. Semivrazhskaya, S. Aroua, M. Yulikov, A. Romero-Rivera, S. Stevenson, M. Garcia-Borràs, S. Osuna and Y. Yamakoshi, *J. Am. Chem. Soc.*, 2020, **142**, 12954–12965.
10 Y. Chai, X. Liu, B. Wu, L. Liu, Z. Wang, Y. Weng and C. Wang, *J. Am. Chem. Soc.*, 2020, **142**, 4411–4418.
11 O. Semivrazhskaya, A. Romero-Rivera, S. Aroua, S. I. Troyanov, M. Garcia-Borràs, S. Stevenson, S. Osuna and Y. Yamakoshi, *J. Am. Chem. Soc.*, 2019, **141**, 10988–10993.
12 S. Yang, M. Chen, R. Guan, B. Li, L. Yang, C. Niu, P. Jin and G.-W. Wang, *Angew. Chem., Int. Ed.*, 2021, **60**, 7880–7886.
13 Y. García-Rodeja, M. Solà and I. Fernández, *J. Org. Chem.*, 2018, **83**, 3285–3292.
14 M. Yamada, Y. Tanabe, J.-S. Dang, S. Sato, N. Mizorogi, M. Hachiya, M. Suzuki, T. Abe, H. Kurihara, Y. Maeda, X. Zhao, Y. Lian, S. Nagase and T. Akasaka, *J. Am. Chem. Soc.*, 2016, **138**, 16523–16532.
15 F.-F. Li, A. Rodríguez-Fortea, J. M. Poblet and L. Echegoyen, *J. Am. Chem. Soc.*, 2011, **133**, 2760–2765.
16 F.-F. Li, A. Rodríguez-Fortea, P. Peng, G. A. Campos Chavez, J. M. Poblet and L. Echegoyen, *J. Am. Chem. Soc.*, 2012, **134**, 7480–7487.
17 N. B. Shustova, A. A. Popov, M. A. Mackey, C. E. Coumbe, J. P. Phillips, S. Stevenson, S. H. Strauss and O. V. Boltalina, *J. Am. Chem. Soc.*, 2007, **129**, 11676–11677.
18 N. B. Shustova, D. V. Peryshkov, I. V. Kuvychko, Y.-S. Chen, M. A. Mackey, C. E. Coumbe, D. T. Heaps, B. S. Confait, T. Heine, J. P. Phillips, S. Stevenson, L. Dunsch, A. A. Popov, S. H. Strauss and O. V. Boltalina, *J. Am. Chem. Soc.*, 2011, **133**, 2672–2690.
19 S. Yang, C. Chen, M. Jiao, N. B. Tamm, M. A. Lanskikh, E. Kemnitz and S. I. Troyanov, *Inorg. Chem.*, 2011, **50**, 3766–3771.
20 F. Jin, N. B. Tamm, S. I. Troyanov and S. Yang, *J. Am. Chem. Soc.*, 2018, **140**, 3496–3499.
21 A. Nakagawa, M. Nishino, H. Niwa, K. Ishino, Z. Wang, H. Omachi, K. Furukawa, T. Yamaguchi, T. Kato, S. Bandow, J. Rio, C. Ewels, S. Aoyagi and H. Shinohara, *Nat. Commun.*, 2018, **9**, 3073.
22 C. Shu, C. Slebodnick, L. Xu, H. Champion, T. Fuhrer, T. Cai, J. E. Reid, W. Fu, K. Harich, H. C. Dorn and H. W. Gibson, *J. Am. Chem. Soc.*, 2008, **130**, 17755–17760.
23 L. Bao, M. Chen, C. Pan, T. Yamaguchi, T. Kato, M. Olmstead, A. Balch, T. Akasaka and L. Xing, *Angew. Chem., Int. Ed.*, 2016, **55**, 4242–4246.
24 L. Feng, T. Nakahodo, T. Wakahara, T. Tsuchiya, Y. Maeda, T. Akasaka, T. Kato, E. Horn, K. Yoza, N. Mizorogi and S. Nagase, *J. Am. Chem. Soc.*, 2005, **127**, 17136–17137.
25 M. Chen, L. Bao, M. Ai, W. Shen and X. Lu, *Chem. Sci.*, 2016, **7**, 2331–2334.
26 W. Shen, L. Yang, Y. Wu, L. Bao, Y. Li, P. Jin, H. Fang, Y. Xie and X. Lu, *J. Org. Chem.*, 2019, **84**, 606–612.
27 Y.-P. Xie, C. Pan, L. Bao, Z. Slanina, T. Akasaka and X. Lu, *Organometallics*, 2019, **38**, 2259–2263.
28 W.-W. Chang, Z.-J. Li, W.-W. Yang and X. Gao, *Org. Lett.*, 2012, **14**, 2386–2389.
29 T. Cai, C. Slebodnick, L. Xu, K. Harich, T. E. Glass, C. Chancellor, J. C. Fettinger, M. M. Olmstead, A. L. Balch, H. W. Gibson and H. C. Dorn, *J. Am. Chem. Soc.*, 2006, **128**, 6486–6492.
30 Y.-Y. Xu, H.-R. Tian, S.-H. Li, Z.-C. Chen, Y.-R. Yao, S.-S. Wang, X. Zhang, Z.-Z. Zhu, S.-L. Deng, Q. Zhang, S. Yang, S.-Y. Xie, R.-B. Huang and L.-S. Zheng, *Nat. Commun.*, 2019, **10**, 485.
31 Y. Maeda, M. Kimura, C. Ueda, M. Yamada, T. Kikuchi, M. Suzuki, W.-W. Wang, N. Mizorogi, N. Karousis, N. Tagmatarchis, T. Hasegawa, M. M. Olmstead, A. L. Balch, S. Nagase and T. Akasaka, *Chem. Commun.*, 2014, **50**, 12552–12555.
32 J. R. Pinzón, D. C. Gasca, S. G. Sankaranarayanan, G. Bottari, T. Torres, D. M. Guldi and L. Echegoyen, *J. Am. Chem. Soc.*, 2009, **131**, 7727–7734.
33 A. G. Avent, P. R. Birkett, A. D. Darwish, S. Houlton, R. Taylor, K. S. T. Thomson and X.-W. Wei, *J. Chem. Soc., Perkin Trans. 2*, 2001, 782–786.

34 L.-L. Deng, S.-L. Xie, C. Yuan, R.-F. Liu, J. Feng, L.-C. Sun, X. Lu, S.-Y. Xie, R.-B. Huang and L.-S. Zheng, *Sol. Energy Mater. Sol. Cells*, 2013, **111**, 193–199.
35 G. A. Olah, I. Bucsi, C. Lambert, R. Aniszfeld, N. J. Trivedi, D. K. Sensharma and G. K. S. Prakash, *J. Am. Chem. Soc.*, 1991, **113**, 9385–9387.
36 E. A. Khakina, O. g. A. Kraevaya, M. L. Popova, A. S. Peregudov, S. I. Troyanov, A. V. Chernyak, V. M. Martynenko, A. V. Kulikov, D. Schols and P. A. Troshin, *Org. Biomol. Chem.*, 2017, **15**, 773–777.
37 H. Ueno, K. Uchiyama, Y. Ma, K. Watanabe, K. Yoza, Y. Matsuo and H. Moriyama, *J. Org. Chem.*, 2018, **83**, 10655–10659.
38 N. Lou, Y. Li and L. Gan, *Angew. Chem., Int. Ed.*, 2017, **56**, 2403–2407.
39 Z. Jia, Q. Zhang, Y. Li, L. Gan, B. Zheng, G. Yuan, S. Zhang and D. Zhu, *Tetrahedron*, 2007, **63**, 9120–9123.
40 K. M. Kadish, X. Gao, O. Gorelik, E. Van Caemelbecke, T. Suenobu and S. Fukuzumi, *J. Phys. Chem. A*, 2000, **104**, 2902–2907.
41 X.-X. Yan, B. Li, H.-S. Lin, F. Jin, C. Niu, K.-Q. Liu, G.-W. Wang and S. Yang, *Research*, 2020, **2020**, 2059190.
42 M. Mikawa, H. Kato, M. Okumura, M. Narazaki, Y. Kanazawa, N. Miwa and H. Shinohara, *Bioconjugate Chem.*, 2001, **12**, 510–514.
43 J. Zhang, Y. Ye, Y. Chen, C. Pregot, T. Li, S. Balasubramaniam, D. B. Hobart, Y. Zhang, S. Wi, R. M. Davis, L. A. Madsen, J. R. Morris, S. M. LaConte, G. T. Yee and H. C. Dorn, *J. Am. Chem. Soc.*, 2014, **136**, 2630–2636.
44 G. M. Sheldrick, *Program for crystal structure solution*, University of Göttingen, Germany, 1997.
45 N. Alegret, A. Rodríguez-Fortea and J. M. Poblet, *Chem.–Eur. J.*, 2013, **19**, 5061–5069.
46 A. Rodríguez-Fortea, J. M. Campanera, C. M. Cardona, L. Echegoyen and J. M. Poblet, *Angew. Chem., Int. Ed.*, 2006, **45**, 8176–8180.